

Supporting Information

Table of contents

S1	Fabrication methods and equipment
S2	3-D models of an inclusion complex and of an unspecifically-bound NP aggregate
S3	Additional TEM images, EF-TEM and STEM data
S4	Statistical analysis of the formation of inclusion complexes
S5	Statistics of the dimensions of SiO ₂ nanocup
S6	Statistical analysis of inclusion depth of the Au NP within a SiO ₂ nanocup
S7	Tilt series of a 1:1 Au NP@SiO ₂ nanocup inclusion complex
S8	Tilt series of an empty SiO ₂ nanocup
S9	Beam damage under TEM
S10	Terminology of an “inclusion complex”
S11	Additional references on related work

S1. Fabrication methods and equipment

Preparation of the Au NP array (BCML)

The hexagonal array of gold nanoparticles (Au NPs) was prepared using block copolymer micellar nanolithography (BCML) as previously reported.^[1] Briefly, polystyrene (1056)-block-poly (2-vinylpyridine)(495) was dissolved in toluene at a concentration of 4 mg/mL and stirred overnight. To the polymer solution, HAuCl₄•3H₂O powder was added at a molar ratio of 0.5 per vinylpyridine unit and stirred overnight to yield self-assembled micelles loaded with HAuCl₄ in the cores. The micelles were then transferred as a uniform monolayer onto the piranha cleaned silicon wafer by spin coating techniques. After that, the wafer was treated under W10 plasma (350W, 0.4mbar) for 45 min. In this step, the polymer shell was removed and HAuCl₄ was reduced, forming a regular quasi-hexagonal array of 8 nm Au NPs separated by 103 nm (as measured by SEM with an in-lens detector).

Growth of metallic silver on the Au NP seeds (Tollens Reaction)

Growth of metallic silver on the Au NP seeds was carried out by an electroless deposition procedure based on the Tollens reaction.^[2] Typically, an Au-NP patterned Si wafer was treated with oxygen plasma (150 W, 0.4 mbar) for 3 min just before the experiment. Tollens reagent was freshly prepared by adding an aqueous solution of NaOH (300 μL, 0.1 M) into an aqueous solution of AgNO₃ (4 mL, 0.25 M) under vigorous stirring. Black solids of Ag₂O were formed. Aqueous ammonia (28%) was added drop wise until all the Ag₂O redissolved to yield a clear solution of [Ag(NH₃)₂]⁺. Generally, ~1.5 – 2 mL of aqueous ammonia is required. Then, growth solution A was prepared by adding the freshly prepared Tollens reagent (3 μL) into 1.5 mL deionized water, while growth solution B was prepared by adding an aqueous solution of glucose (6 μL, 0.1 g/mL) into 1.5 mL deionized water. Growth solutions A and B were mixed quickly and poured over a plasma-treated Au-NP patterned wafer to start the growth process. The thickness of the silver layer is determined by the duration of this growth process, which typically takes ~3 – 6 min. After that, the sample wafer was washed twice with deionized water and dried under a gentle flow of nitrogen.

Deposition of oxide materials (GLAD)

The deposition of the oxide materials (SiO₂, TiO₂ or Al₂O₃) on the Au-Ag JNPs was performed in a vacuum chamber with pressures in the range 10⁻⁷ – 10⁻⁶ torr, by electron-beam evaporation.^[3,4] The substrate was tilted at 85 degree with respect to the flux and was constantly rotating. No substrate cooling was used. The angle of deposition and rotation speed was kept constant during all depositions.

In general, the encapsulated “guest” NPs can be composed of noble metals that are compatible with the BCML scheme, such as Au, Pt and Pd,^[1] while the “host” nanocups can be grown from GLAD-compatible materials, including SiO₂, TiO₂, Al₂O₃, Si and Ti etc. Therefore, our scheme allows a large number of potential materials combinations and thus a considerable range of NP@nanocup inclusion complexes.

Transmission electron microscopy (TEM)

TEM samples were prepared by drop casting $\sim 5 \mu\text{L}$ of nanocolloidal solution onto a Holey[®] carbon coated TEM grid (Cu 400 mesh), followed by drying. The sample loaded TEM grid was then washed (deionized water) to remove excess salts, and finally dried. Bright field TEM images were recorded on a Philips CM200 or a Zeiss 912 Omega under an accelerating voltage of 200 kV or 120 kV, respectively. Energy-filtered TEM (EF-TEM) images were recorded on a Zeiss 912 Omega (120 kV) with the appropriate energy slit inserted into the in-column electron energy filter. Background signals of each elemental core-loss image were measured, modeled and subtracted by the “three-window technique” using the power law model in the Gatan Digital Micrograph program (<http://www.gatan.com/software/>).

HAADF-STEM and STEM-edx

Scanning transmission electron microscopy (STEM) was conducted using Zeiss SESAM under an accelerating voltage of 200 kV. High-angle annular dark field STEM (HAADF-STEM) images and STEM energy dispersive X-ray (STEM-edx) elemental maps were recorded at a tilt angle of 20° to maximize the X-ray signal.

General instruments

TePla PS210 microwave plasma system was used for W10 (10% H₂, 90% Ar) plasma treatment, while PVA TePla PS100 microwave plasma system was used for oxygen plasma treatment.

S2. 3-D models of an inclusion complex and of an unspecifically-bound NP aggregate

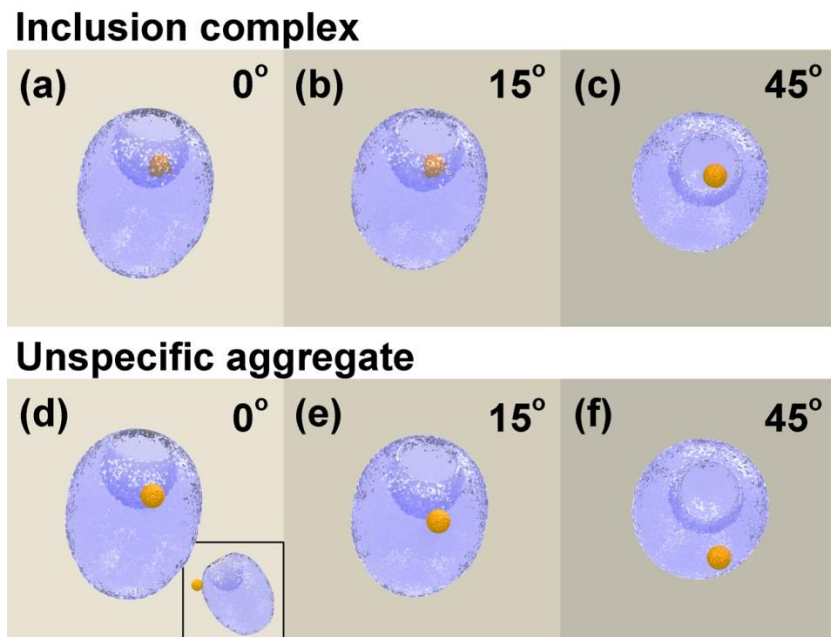


Figure S1. Computer generated 3-D models of the inclusion complex and an unspecifically-bound NP aggregate. (a)–(c) Snapshots of the inclusion complex taken at various tilt angles. The projected image of the encapsulated Au NP overlaps with that of the cavity regardless of the tilt angle. (d) – (f) Snapshots of the unspecific aggregate taken at different tilt angles. It is noted (inset of (d)) that in the case of the unspecific aggregate, the Au NP is adsorbed on the outer surface of the nanocup, but not inside the cavity of the nanocup. Although projected images of the inclusion complex and the unspecific aggregate can appear to be very similar at low tilt angles, the difference becomes apparent at higher tilt angles where the Au NP projection no longer overlaps with that of the cavity in the case of the aggregate. In addition, the Au NP projection of the unspecific aggregate also shows a larger relative displacement upon tilting, as the Au NP is further away from the center of the empty nanocup.

S3. Additional TEM images, EF-TEM and STEM data

Transmission electron microscopy (TEM) images of a typical 1:1 Au NP@SiO₂ nanocup inclusion complex are shown in Figure S2. The negligible relative displacement of the Au NP in the tilt-series reveals that the Au NP is indeed encapsulated deep inside the nanocup cavity.

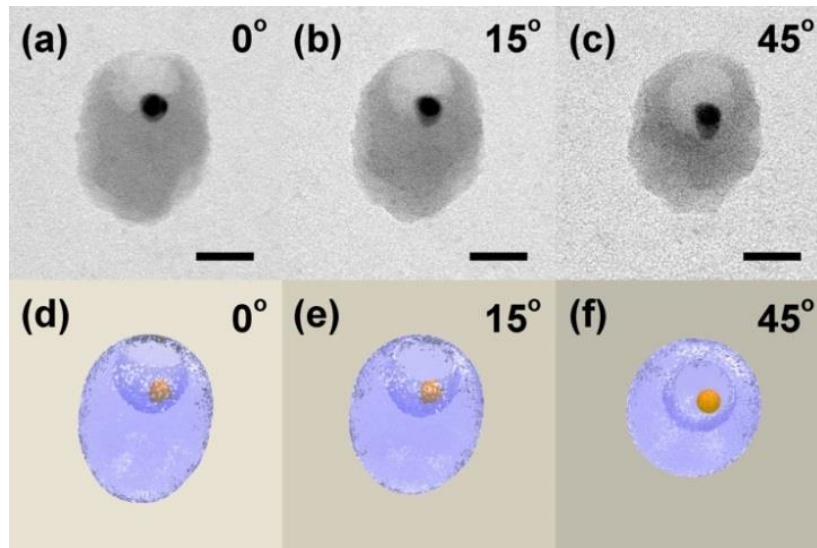


Figure S2. (a) - (c) Transmission electron micrographs of a typical 1:1 Au NP@SiO₂ nanocup inclusion complex at various tilt angles; (d) - (f) corresponding snapshots of a computer-generated 3-D model of the complex. Scale bars = 20 nm.

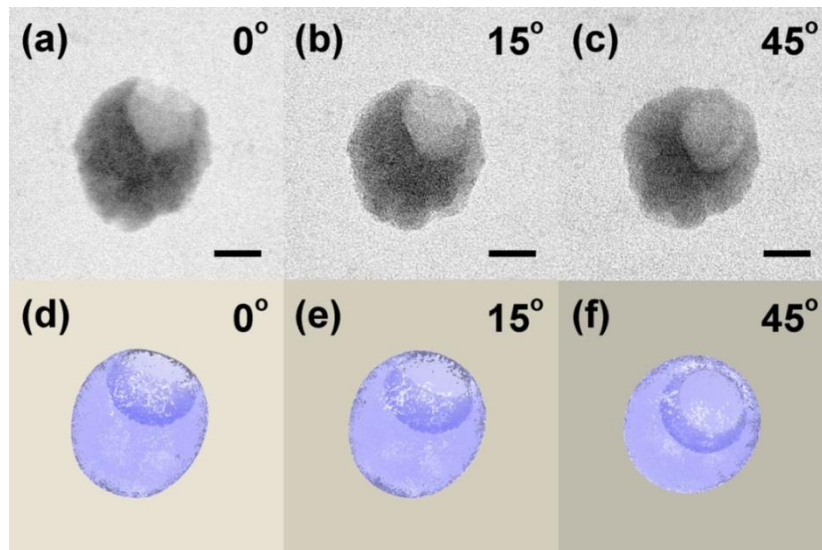


Figure S3. (a) - (c) Transmission electron micrographs of an empty SiO₂ nanocup at various tilt angles; (d) - (f) corresponding snapshots of a computer-generated 3-D model for the SiO₂ nanocup. Scale bars = 20 nm.

Energy-filtered TEM (EF-TEM) was used to generate elemental maps of both the Au-Ag-SiO₂ d-JNP intermediate and the Au NP@SiO₂ nanocup inclusion complex. The elemental maps of the d-JNP show the tight encapsulation of Au by Ag and that of Ag by SiO₂ (Figure S4 a-c). The presence and location of the Au NP can be induced from the drop of the Ag or Si signal intensity in the elemental maps of the d-JNP and the inclusion complex, respectively, which is in good agreement with the expected size and position of the Au NP (Figure S4c, drop marked by a black arrow). After the oxidation step, no Ag signal can be detected on top of that of the background noise in the inclusion complex (Figure S4 d-f), and there is a clear formation of a cavity, as illustrated by the drop of the Si signal in the region where the Ag was previously found. It is noted that in the lower part of this cavity, the Au NP appears as a round black dot.

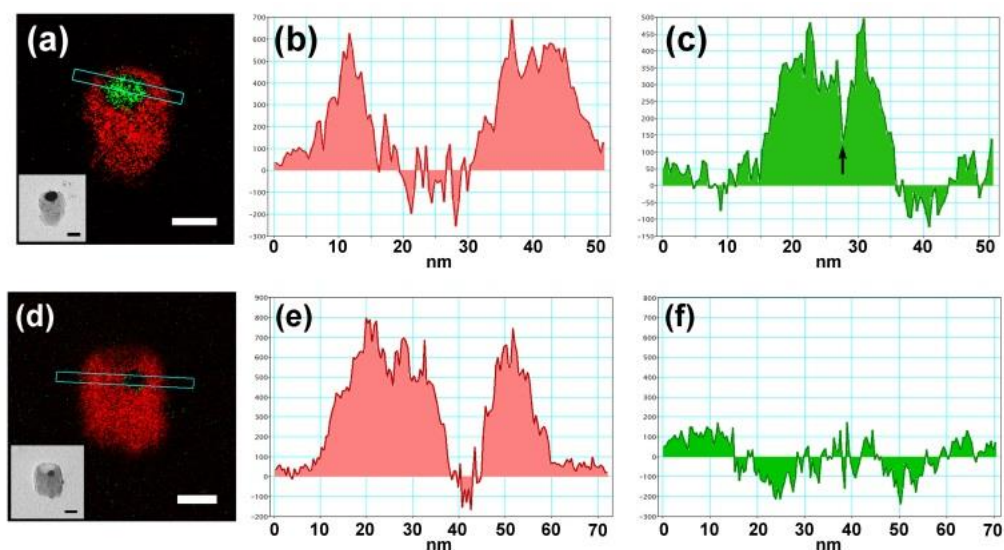


Figure S4. Energy-filtered TEM (EF-TEM) analysis of (a) – (c) an Au-Ag-SiO₂ d-JNP and (d) – (e) an Au NP@SiO₂ nanocup inclusion complex. (a), (d) False-color elemental map. Inset: bright-field TEM image of the same region of interest. Scale bars = 20 nm. Color scheme (corresponding core-loss edges): red – silicon (Si L2, 3), green – silver (Ag M4, 5). Profiles of the (b), (e) silicon and (c), (f) silver maps across the d-JNP and the inclusion complex as indicated by the cyan rectangles in (a) and (d), respectively. The dip in signal intensity in the silver profile (marked by a black arrow in (c)) reveals the position of the embedded Au NP.

Inclusion complexes of TiO₂ and Al₂O₃ nanocups

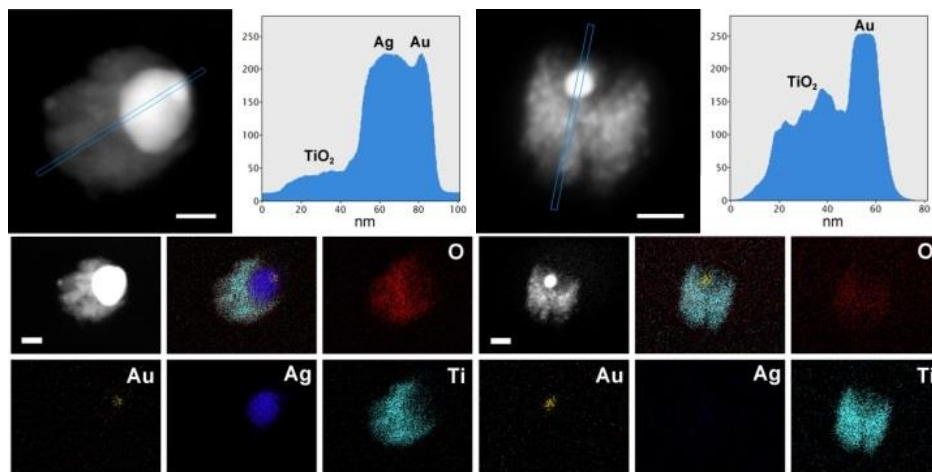


Figure S5. HAADF-STEM (Z-contrast) images of a typical (a) Au-Ag-TiO₂ d-JNP, (b) Au NP@TiO₂ nanocup inclusion complex. Corresponding intensity line profiles (blue frames denote the area of integration) are on the right for each of the Z-contrast images. STEM-edx elemental maps are shown below each of the corresponding HAADF-STEM images. All scale bars are 20 nm. Color code (and the corresponding transition edges): yellow, gold (Au L); blue, silver (Ag L); cyan, titanium (Ti K); red, oxygen (O K); pink, platinum (Pt L); green, silicon (Si K).

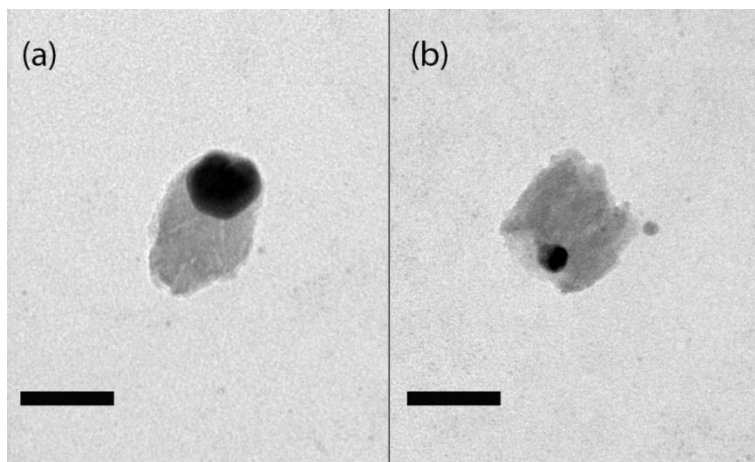


Figure S6. (a) Au-Ag-Al₂O₃ d-JNP and (b) Au NP@ Al₂O₃ nanocup inclusion complex. Here Al₂O₃, rather than SiO₂, was grown on top of the Au-Ag JNP seeds in the GLAD process, while oxidative dissolution of metallic silver will then yield the desired product. Scale bars are 50nm.

S4. Statistical analysis of the formation of inclusion complexes

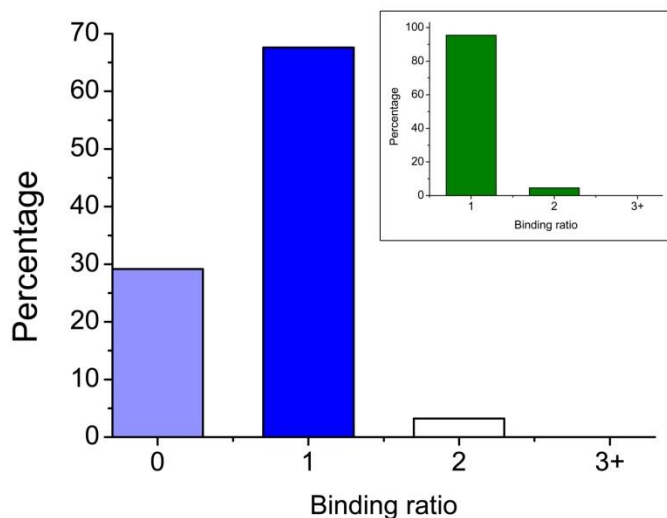


Figure S7. Histogram showing the percentage of empty nanocups (binding ratio = 0) and inclusion complexes of different binding ratios in a typical sample of Au NP@SiO₂ nanocup inclusion complexes. Inset showing the percentage of inclusion complexes of different binding ratios within the population of inclusion complexes. Statistical analysis is based on 500 particles.

Formation of 2:1 Au NP@SiO₂ nanocup inclusion complexes is believed to be due to the presence of dimeric Au NP seeds that were formed in the BCML process (see Figure 2 in the main text). This is supported by the observation that the percentage of the dimeric Au NPs in the BCML sample is very similar to that of the inclusion complexes with a 2:1 binding ratio. Inclusion complexes with 3 or more encapsulated Au NPs, as well as unspecific aggregates with empty nanocups, are not observed, indicating that Au NP “guest” exchange/transfer between nanocup “hosts” is a rare event.

S5. Statistics of the dimensions of SiO₂ nanocups

Table S1. Dimensions of the SiO₂ nanocups and the encapsulated Au NPs; mean \pm standard deviation in nm is shown. Statistics is based on measurements on 200 particles in bright-field TEM images.

Cavity depth	Cavity width	Opening width	Wall thickness at opening	Particle size	Au NP size
21.9 \pm 3.2	26.2 \pm 3.8	24.8 \pm 3.8	5.1 \pm 1.0	45.5 \pm 6.8	8.5 \pm 0.9

Accurate measurements are difficult to obtain for some of the dimensions unlike in the case of highly symmetric convex NPs. Although most of the particles were found to be “lying flat” on the TEM grid, where the angle between the principle C_∞ axis of the nanocup and the plane of the grid is relatively small, the dimensions of the projected image still suffer from considerable variations owing to a small but non-constant inclination of the particle. While measurements are based on the projected images, the standard deviation of the actual dimensions is expected to be even smaller.

The cavity dimensions are well controlled, with a standard deviation under 15%, demonstrating a high structural fidelity of our nanocups (Figure 3). It is noted that the dimensions of the nanocup cavity match well with that of the Au-Ag JNPs as determined by both scanning electron microscopy (SEM) and TEM. This confirms that by controlling the size of the Au-Ag JNPs in the Tollens growth step, dimensions of the nanocup cavity can be readily fine-tuned to fit a specific application and that no observable damage occurs during the oxidation of metallic silver in solution.

S6. Statistical analysis of inclusion depth of the Au NP within a SiO₂ nanocup

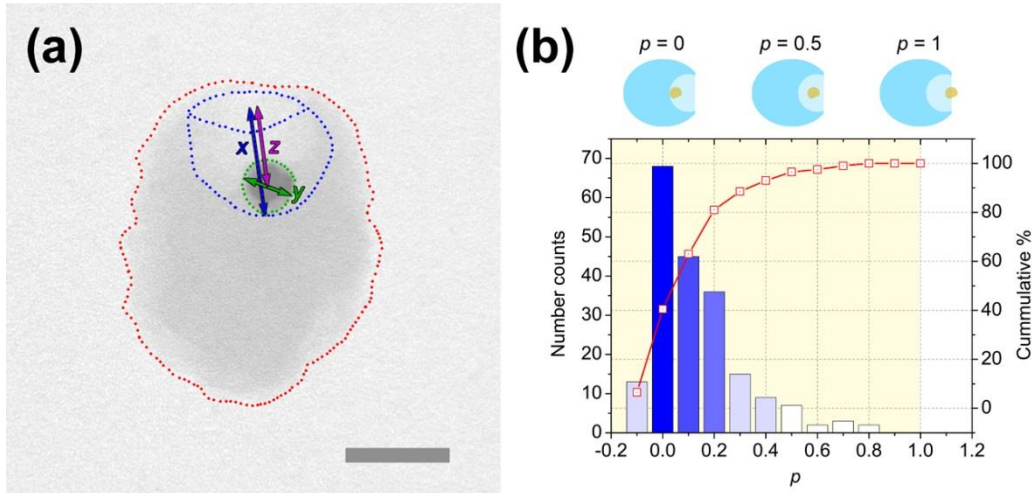


Figure S8. (a) Definition of dimensions in this statistical study. (b) Statistics of relative inclusion depth p based on 200 inclusion complexes (See below). The histogram corresponds to the frequency of the position of the Au NP inside the nanocups. The red curve shows the cumulative percentage of NPs located at the different positions within the nanocup.

Cavity depth of the nanocup: x (blue arrow in Figure S8a)

Diameter of the encapsulated Au NP: y (green arrow in Figure S8a)

Depth of the center of the AuNP inside the cavity: z (purple arrow in Figure S8a)

Maximum possible $z = z_{\max} = x - 0.5y$

Relative depth of the Au NP inside the cavity $p = 1 - (z / z_{\max}) = 1 - (z / (x - 0.5y))$

1. When $z = z_{\max}$, $p = 0$ (Au NP achieved its maximum possible depth inside the cavity)
2. When $0 < z < z_{\max}$, $1 > p > 0$ (Au NP is encapsulated inside the cavity, indicated by the light yellow area in Figure S8b)
3. When $z = 0$, $p = 1$ (Center of the Au NP located at the opening of the nanocup)
4. When $z < 0$, $p > 1$ (Au NP located outside the nanocup); this population of “empty nanocups” is not included in this statistical study.

Statistics based on 200 inclusion complexes reveals the following:

1. Mean value of $p = 0.135$. This indicates that on average Au NPs are encapsulated deep inside the nanocup cavity.
2. >80% of the inclusion complexes are having $p \leq 0.2$
3. >95% of the inclusion complexes are having $p \leq 0.5$

S7. Tilt series of a 1:1 Au NP@SiO₂ nanocup inclusion complex

Figure S9. The aligned bright-field TEM tilt series of a 1:1 Au NP@SiO₂ nanocup inclusion complex is appended as an animated gif file, and can be downloaded as part of the supporting information. Tilt angle: -60° to 55° with a resolution of 5°. Magnification: 480 kx. Scale bar = 20 nm.

S8. Tilt series of an empty SiO₂ nanocup

Figure S10. The aligned bright-field TEM tilt series of an empty SiO₂ nanocup is appended as an animated gif file, and can be downloaded as part of the supplementary information. Tilt angle: -60° to 0° with a resolution of 5°. Magnification: 480 kx. Scale bar = 20 nm.

It is noted that a slight change in cavity dimensions is induced upon prolonged (>60 mins) electron beam irradiation (See section S9). The change is particularly significant in the case of empty SiO₂ nanocups.

S9. Beam damage under TEM

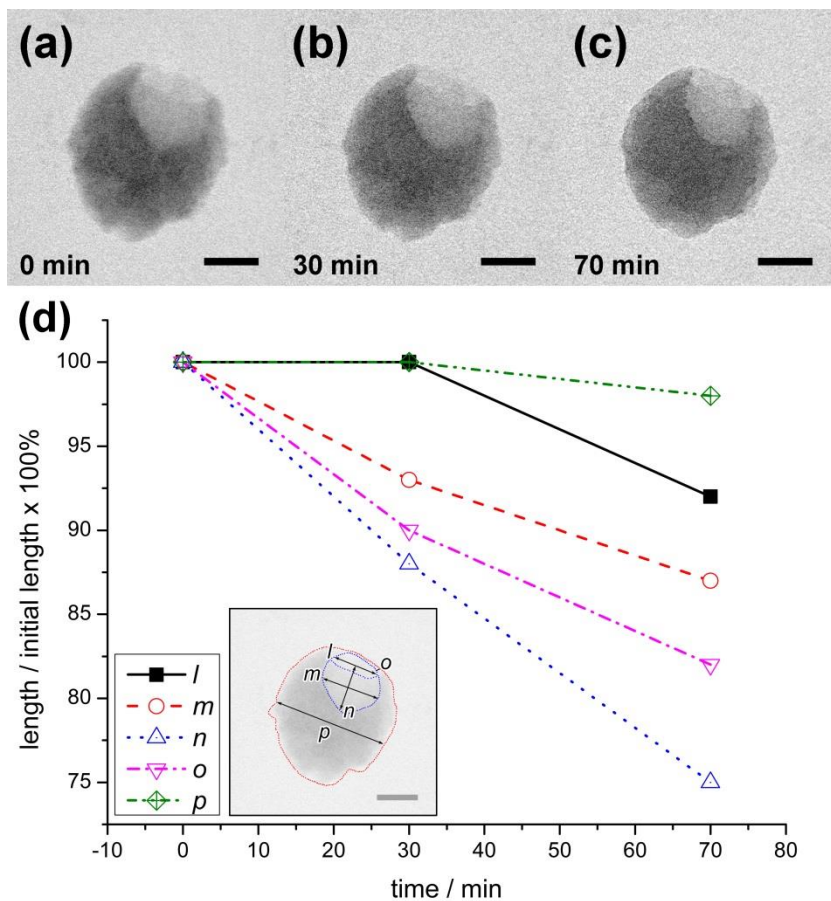


Figure S11. Beam damage of an empty SiO₂ nanocup under an accelerating voltage of 200 kV and typical bright-field TEM imaging conditions. (a) – (c) Time-lapsed TEM images, scale bars = 20 nm. (d) Graph showing the decrease in dimensions caused by electron beam irradiation. Inset: definitions of dimensions measured.

S10. Terminology of an “inclusion complex”

As pointed out by a helpful referee, it is important to discuss the reversibility of inclusion complexes. We therefore want to stress that the inclusion complexes of this paper, similar to a few other known molecular “inclusion complexes”, show no reversibility for the present experimental conditions.

Based on the principle of microscopic reversibility, all supramolecular complexation events must be reversible. However, under ambient conditions it is not always possible to observe the reverse (unbinding) reaction. In these cases the term “host-guest inclusion complex” is only defined by the structure and topology of the complex but not by the kinetics. A classical example of such an “irreversible” inclusion complex is a “carceplex” where a guest molecule is irreversibly encapsulated inside the carcerand host.^[5] At the other extreme are host-guest inclusion complexes that are so dynamic that the hosts only form in the presence of the complementary guests (templates) and cannot exist individually.^[6]

In the case of our Au NP@SiO₂ nanocup inclusion complexes, the Au NP guest is pre-organised in the form of a Au-Ag-SiO₂ double Janus NP, and then kinetically encapsulated at the bottom of the SiO₂ nanocup cavity upon dissolution of Ag. The encapsulated Au NP guests can be released by external trigger to yield stable empty nanocup hosts. Although this binding-release event is irreversible, the structure itself does meet the condition of an “inclusion complex”, if one applies the arguments as discussed above. In addition, the triggered release of the Au NP guest demonstrates the controllable dynamics and the supramolecular nature of our inclusion complexes. Meanwhile, efforts in our labs are made to realise the full binding reversibility of our inclusion complexes.

S11. Additional references on related work

Nanoparticles with concave faces

- H. Zhang, M. S. Jin, J. G. Wang, W. Y. Li, P. H. C. Camargo, M. J. Kim, D. R. Yang, Z. X. Xie, Y. Xia, *J. Am. Chem. Soc.* **2011**, *133*, 6078–6089.
- M. S. Jin, H. Zhang, Z. X. Xie, Y. Xia, *Angew. Chem. Int. Ed.* **2011**, *50*, 7850–7854; *Angew. Chem.* **2011**, *123*: 7996–8000.

Cap shaped nanoparticles

- C. George, D. Dorfs, G. Bertoni, A. Falqui, A. Genovese, T. Pellegrino, A. Roig, A. Quarta, R. Comparelli, M. L. Curri, R. Cingolani, L. Manna, *J. Am. Chem. Soc.* **2011**, *133*, 2205–2217.
- D. Jagadeesan, U. Mansoori, P. Mandal, A. Sundaresan, M. Eswaramoorthy, *Angew. Chem. Int. Ed.* **2008**, *47*, 7685–7688; *Angew. Chem.* **2008**, *120*, 7799–7802.

References

- [1] R. Glass, M. Möller, J. P. Spatz, *Nanotechnology* **2003**, *14*, 1153–1160.
- [2] S. Kruss, V. Srot, P. A. van Aken, J. P. Spatz, *Langmuir* **2012**, *28*, 1562–1568.
- [3] M. M. Hawkeye, M. J. Brett, *J. Vac. Sci. Technol. A* **2007**, *25*, 1317–1335.
- [4] A. G. Mark, J. G. Gibbs, T.-C. Lee, P. Fischer, *Nat. Mater.* **2013**, *12*, 802–807.
- [5] D. Cram, S. Karbach, Y. H. Kim , L. Baczynskyj , G. W. Kallemeyn, *J. Am. Chem. Soc.*, **1985**, *107*, 2575–2576.
- [6] D. Ajami, J. Rebek, Jr, *Proc. Natl. Acad. Sci. U.S.A.*, **2007**, *104*, 16000–16003.